# Electrocardiogram signal classification for automated delineation using bidirectional long short-term memory

Siti Nurmaini [a,*], Alexander Edo Tondas [b], Annisa Darmawahyuni [a],
Muhammad Naufal Rachmatullah [a], Jannes Effendi [a], Firdaus Firdaus [a], Bambang Tutuko [a]

[a] *Intelligent System Research Group, Universitas Sriwijaya, Palembang, 30139, Indonesia*
[b] *Department of Cardiology & Vascular Medicine, Dr. Mohammad Hoesin Hospital, Palembang, Indonesia*

ARTICLE INFO

ABSTRACT

Analysis of electrocardiogram (ECG) signals is challenging due to the complexity of their signal morphology. Any irregularity in a cardiac rhythm can change the ECG waveform. A reliable machine learning model is developed here to provide substantial input to cardiologists and help confirm their diagnoses. To achieve high diagnostic accuracy, nearly all ECG analytics tools require records of the positions and morphologies of various segments of P-waves, QRS complexes, and T-waves to be kept in ECG records. However, analyzing such vast amounts of ECG records is not always easy. In most cases, it is challenging and highly time-consuming. Hence, an in-depth investigation regarding automatic ECG signal delineation is necessary. This paper proposes an automated delineation algorithm for ECG waveform signals that utilizes recurrent neural networks (RNNs) with bidirectional long short-term memory (LSTM) architecture. This delineation process consists of four steps: noise cancellation, ECG waveform segmentation, ECG signal classification in four classes (P-wave, QRS complex, T-wave, and isoelectric line) and model evaluation. The classification is conducted based on time duration, and each waveform is determined by using annotated data from the well-known QT database (QTDB). The results show that the proposed model produces satisfactory performance for the four classes in terms of average accuracy, sensitivity, specificity, precision, and F1-score, with values of 99.64%, 98.74%, 99.75%, 98.81%, and 98.78%, respectively. The proposed model is validated with abnormal ECG signals from the QTDB, i.e., MIT-BIH Arrhythmia, MIT-BIH ST Change, MIT-BIH Supraventricular Arrhythmia, European ST-T, and MIT-BIH Long-Term ECG. The results show that bidirectional LSTM can delineate ECG signals from QTDB in both normal and abnormal conditions. The proposed delineation method could be utilized in potential applications following further investigation.

## 1. Introduction

The electrocardiogram (ECG) is an electrophysiological signal that contains a large amount of valuable information about the electrical activity of the heart. ECG waveforms are seen in clinical assessments of heartbeats and include P-waves, QRS complexes, and T-waves [1,2]. The amplitudes and time intervals of ECG waveforms provide insight on heart rhythm abnormalities and heart diseases such as ischemia, QT syndrome (long and short), and myocardial infarction [2–4]. ECG waveform delineation is utilized for determining characteristics such as amplitudes and time intervals. Performing an accurate delineation, however, is quite a difficult task for many reasons: (i) P-waves have low amplitudes and can be obscured by electrode motion or muscle noise [2]; (ii) P- and T-waves can be biphasic, which increases the difficulty of accurately determining the starting points or endpoints of the waves [2]; (iii) P-waves can be absent, although they can also partially overlap with the T-waves from the previous beat in rapid heart rate patterns [3]; and (iv) some arrhythmia entities cannot contain all the standard ECG waves [5]. The start of the wave is the initial onset of the signal, while the end of the wave is the offset of the signal. Therefore, designing an automated and accurate ECG delineation would be useful for making good decisions about heart rhythm abnormalities.

The importance of an automatic delineation algorithm is that it recognizes the individual waveform components of P-waves, QRS complexes, and T-waves. These signal recognition processes include the ECG positions (onset, peak, and offset) and the magnitudes from all waveform components [5]. In previous studies, the automated delineation of ECG signals was widely performed in a way that aimed to measure the width or duration of the waves [6,7]. However, the starting and ending points of the durations were very complicated and difficult to measure. Due to this, it always appears in well-known and distinguishable frequency bands. Several automated methods for making such measurements have been proposed, such as linear regression, logistic regression, and classification [3,4,8,9]. Regression was the most prominent method, as it was utilizable when all the attributes were numeric, while classification was used when all the attributes were categories. However, the ability of the two methods to draw boundaries between the two classes was restricted at some points. An essential challenge is to find more than one boundary to partition the set. Several algorithms have been proposed in the literature to accomplish this, including threshold-based algorithms [10], hidden Markov models [11], curve fitting [12], wavelet transforms [13], and machine learning techniques [3,14,15]. For most current algorithms, the typical strategy is to extract the P-waves, QRS complexes, and T-waves. The accuracy of the overall device, therefore, depends greatly on the accuracy of the segmentation of the ECG and the measurement of its features. However, due to the subjective nature of the measurements in the segmentation and measurement phases, there is always a high degree of uncertainty and variability. Thus, designing and developing an automated delineation algorithm for ECG signals in a robust condition is a crucial process [16].

Several studies have been undertaken to evaluate the performance of these algorithms. Unfortunately, there is a lack of standardized databases containing a reasonably large number of carefully annotated heartbeats with manually performed waveform boundary measurements. This situation reflects the enormous effort a clinician must undertake to manually annotate a statistically relevant collection of QRS complexes. Deep learning (DL) with automated feature learning allows multi-layered computational models based on traditional neural networks to learn from multi-level abstraction representations of data [17]. DL is a relatively new approach, but in many healthcare applications, it has shown a promising capacity for data synthesis [18–20]. Neural networks are used for complex cardiological tasks—in particular, detection of heartbeats in arrhythmia [8], discrimination between hypertrophic functional and pathological remodeling patterns [21], risk stratification and heart failure prognosis [22], and various implementations of ECG analysis [23,24].

To the best of our knowledge, studies of DL application in automated delineation for detecting and predicting P-waves, QRS complexes, and T-waves are still limited. In contrast, ECG waveform signal delineation needs to be accurately performed. In this study, we present the idea of performing automated delineation by using DL. The delineation of ECG waveforms only focuses on identifying ECG cardiac waves. Hence, the design and development of an automated delineation algorithm for ECG waveform signals using DL were needed to investigate the issue in greater depth. Among DL architectures, recurrent neural networks (RNNs) are one type of architecture that can model a sequence of data, e. g., in ECG signal processing. RNNs can be implemented for sequential prediction to model the flow of time directly. RNNs and their variants (long short-term memory (LSTM) and gated recurrent units (GRUs)) can be improved in aspect, as their performance can be optimized by providing the classifier with crafted features [25]. However, in some cases, LSTM performs better than GRU [25,26]. Hence, accurate ECG delineation using RNNs with LSTM architectures is desirable. One of the characteristics of an ECG signal is its sequence. The sequence of an ECG signal detects and records the strength and timing of the electrical activity occurring in a person's heart. RNNs with LSTM architectures have a powerful architecture that has been successfully and accurately implemented for ECG delineation [27]. Therefore, by combining the advantages of RNNs with LSTM architectures and the characteristics of ECG signals, this paper uses RNNs with LSTM architectures as a method for delineating ECG signals. The contributions and novelties of the paper are as follows:

- ECG signal waveforms were classified for automating delineation from the start of a P-wave to the start of the next P-wave;
- Each sample was classified into four durations of cardiac waves—P-waves, QRS complexes, T-waves, and isoelectric lines—to produce the identification of temporal features;
- The bidirectional LSTM architecture was used for classification;
- The signal delineation is evaluated for normal and abnormal QTDB datasets.

The rest of this paper is organized as follows. In Section 2, we explain the methods used in this research. We present our results and a discussion in Section 3 and evaluate the performance of our proposed method in Section 4. Finally, we review our conclusions in section 5.

## 2. Methods

### 2.1. Discrete wavelet transform

ECG signals are typically distorted by different forms of signal noise, including artifacts such as power lines; the most common of these are highlighted in Ref. [28]. This noise affects the quality of the signal and decreases the accuracy of interpretation. Because of the noise and interference, information of interest cannot easily be extracted from the raw signal, which must initially be processed before generating a model for ECG interpretation [29–32]. To achieve the purpose of denoising ECG signals, this paper uses a wavelet transform (WT). The wavelet transform, especially the wavelet package decomposition (WPD), can be separated into high- and low-frequency content in noisy signals [33]. The wavelet analysis was applied to specific biomedical engineering problems, including reducing noise in ECG signals [28,34]. Wavelet transformation is a time-frequency technique that represents local ECG signal information in the time and frequency domains to change the low-frequency and high-frequency sub-bands separately through time window and frequency window settings [35]. The denoising wavelet algorithm comprises three steps: decomposition of the wavelet, coefficient processing, and wavelet reconstruction [36]. The discrete wavelet transforms (DWT) of a one-dimensional signal $f[n]$ can be calculated by simultaneously passing it through a high-pass and a low-pass filter. If a low-pass filter has the impulse response $g[n]$, then its DWT can be evaluated by calculating the convolution of an original signal with an impulse response defined as follows,

$$y[n] = (f * g)[n] = \sum_{k=-\infty}^{\infty} f[k].g[n-k] \tag{1}$$

The result of the decomposition is filtered again using the soft thresholding method (Equation (1)) with a universal threshold (Equation (2)). The results of the first-level decomposition are used to calculate the threshold value as,

$$t = \sigma\sqrt{2\log N} \tag{2}$$

where $\sigma = \frac{median\,(|cD_j|)}{0.6457}$, and $N$ is length of signal or data (array)

### 2.2. RNNs-LSTM architecture

Artificial neural networks (ANNs) possess two drawbacks: (i) an inability to deal with temporal data, which requires fixed input and output sizes, and (ii) the limitations of networks that cannot address future input based on past input [37]. These drawbacks exist because ANNs are independent and omit everything from previous feed-forward

input. They concentrate only on a particular input and then map it directly to an output vector. The output from sequential input is only significant when all inputs are dependent on each other because the whole input is useful.

In contrast, recurrent neural networks (RNNs) offer more flexibility in processing various input and output sizes by using their memory to produce output that functions dependently based on the entire history of input [38]. RNNs allow modeling to be performed over a sequence or chain of a vector. These sequences can be either input, output, or even both. One of the architectures for RNNs is long short-term memory (LSTM). This architecture was proposed to solve the vanishing or exploding gradient problem, which was addressed by RNNs [26,39]. RNNs with LSTM architecture are appropriate for sequential data processing based on time-steps [40,41]. This study was concerned with the time duration (in seconds) of detecting the onset-offset points of P-QRS-T. The architecture of LSTM is slightly different when compared to the RNNs standard due to the existence of a complicated mechanism called the memory cell. The memory cell learns the input in an intelligent way to enable the LSTM network to process and store the information for short-term and long-term memory. By using the gate mechanism, the memory cell cycle monitors the amount of information from the previous time-step that contributes to the current output based on three components: (1) input, (2) forget, and (3) output gate [26] (Fig. 1). Fig. 1 illustrates the processes of forward pass and backward pass in LSTM architecture based on the previous ($x_{t-1}$), current ($x_t$), and next times ($x_{t+1}$). Both types of pass are described in what follows.

### 2.2.1. Forward pass

The forward pass calculates as input $x$ with a length $T$ by starting $t+1$ and recursively applying an update equation while adding $t$. The scripts $i, f$, and $o$ refer to the input, forget, and output gates from the block, respectively. The script $c$ refers to one of the $C$ memory cells. At the time $t$, LSTM receives a new input in the form of vector $x^t$ (including bias) and the output of the vector $h^{t-1}$ in the previous time-step. The weight of the one cell to input, forget, and output gates annotated as $W_c$, $W_i, W_f$ and $W_o$ respectively. The one cell parameters of the input value, input, forget, and output gates ($a^t, i^t, f^t, o^t$) can be described in equations (3)–(6) as,

$$a^t = tanh\left(W_c x^t + U_c h^{t-1}\right) \tag{3}$$

$$i^t = \sigma\left(W_i x^t + U_i h^{t-1}\right) = \sigma\left(\widehat{i}^t\right) \tag{4}$$

$$f^t = \sigma\left(W_f x^t + U_f h^{t-1}\right) = \sigma\left(\widehat{f}^t\right) \tag{5}$$

$$o^t = \sigma\left(W_o x^t + U_o h^{t-1}\right) = \sigma(\widehat{o}^t) \tag{6}$$

By ignoring non-linearity, all equations (3)–(6) become equation (7) as,

$$z^t = \begin{bmatrix} \widehat{a}^t \\ \widehat{i}^t \\ \widehat{f}^t \\ \widehat{o}^t \end{bmatrix} = \begin{bmatrix} W^c & U^c \\ W^i & U^i \\ W^f & U^f \\ W^o & U^o \end{bmatrix} \cdot \begin{bmatrix} x^t \\ h^{t-1} \end{bmatrix} = W \cdot I^t \tag{7}$$

The memory cell $c^t$ values are updated by combining $a^t$ and the contents of the previous cell $c^{t-1}$. It processes by using the combination of the magnitude of the gate input $i^t$ and forget gate $f^t$. Finally, the LSTM cell calculates the output $h^t$ value by passing an updated cell value through non-linearity ($\odot$ denotes the elementwise product).

$$c^t = i^t \odot a^t + f^t \odot c^{t-1} \tag{8}$$

$$h^t = o^t \odot f(c^t) \tag{9}$$

### 2.2.2. Backward pass

Back-propagation through time (BPTT) is known as backward pass in the LSTM architecture. The backward process differentiates the equation (8) or $\delta c^t = \frac{\partial E}{\partial c^t}$ and equation (9) or $\delta h^t = \frac{\partial E}{\partial h^t}$. By using the *chain rule* equations (8) and (9) become,

$$\frac{\partial E}{\partial o_i^t} = \frac{\partial E}{\partial h_i^t} \odot \frac{\partial h_i^t}{\partial o_i^t} = \delta h_i^t \odot f(c_i^t) \text{ or } \delta o^t = \delta h^t \odot f(c^t) \tag{10}$$

$$\frac{\partial E}{\partial c_i^t} = \frac{\partial E}{\partial h_i^t} \odot \frac{\partial h_i^t}{\partial c_i^t} = \delta h_i^t \odot o_i^t \left(1 - f^2(c_i^t)\right) \text{ or } \delta c^t + = \delta h^t \odot o^t \odot \left(1 - f^2(c^t)\right) \tag{11}$$

The activation function $f$ is used in this phase is Tanh. The sign $+=$ for calculating the gradient, for each time-step $t+1$. Updated the memory cell of LSTM ($a^t, i^t f^t$, and $c^{t-1}$) on equations (3)–(5) respectively in backward pass process as,

$$\frac{\partial E}{\partial a_i^t} = \frac{\partial E}{\partial c_i^t} \odot \frac{\partial c_i^t}{\partial a_i^t} = \delta c_i^t \odot i_i^t \text{ or } \delta a^t = \delta c^t \odot i^t, \tag{12}$$

$$\frac{\partial E}{\partial i_i^t} = \frac{\partial E}{\partial c_i^t} \odot \frac{\partial c_i^t}{\partial i_i^t} = \delta c_i^t \odot a_i^t \text{ or } \delta i^t = \delta c^t \odot a^t, \tag{13}$$

$$\frac{\partial E}{\partial f_i^t} = \frac{\partial E}{\partial c_i^t} \odot \frac{\partial c_i^t}{\partial f_i^t} = \delta c_i^t \odot c_i^{t-1} \text{ or } \delta f^t = \delta c^t \odot c^{t-1}, \tag{14}$$

$$\frac{\partial E}{\partial c_i^{t-1}} = \frac{\partial E}{\partial c_i^t} \odot \frac{\partial c_i^t}{\partial c_i^{t-1}} = \delta c_i^t \odot f_i^t \text{ or } \delta c^{t-1} = \delta c^t \odot f^t \tag{15}$$

To compute the input, forget, and output gate in the backward pass phase, parameter $z^t$ in equation (7) (forward phase) is updated to become $\delta z^t$ by changing all parameters $\delta \widehat{a}^t, \delta \widehat{i}^t, \delta \widehat{f}^t$, and $\delta \widehat{o}^t$ as,
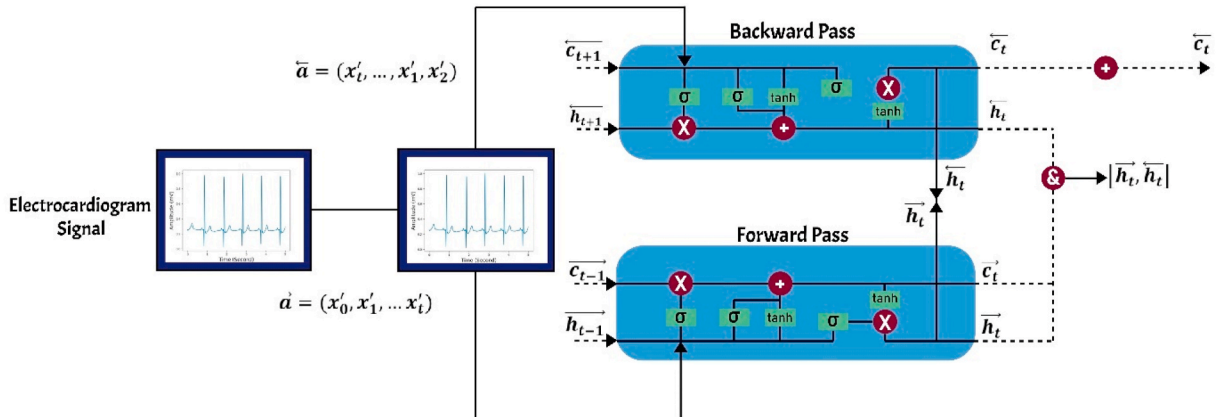


**Fig. 1.** The LSTM architecture based on previous, current and next time.

$$\delta\widehat{a}^t = \delta a^t \odot \left(1 - \tanh^2(\widehat{a}^t)\right) \tag{16}$$

$$\widehat{\delta i}^t = \delta i^t \odot i^t \odot \left(1 - i^t\right) \tag{17}$$

$$\widehat{\delta f}^t = \delta f^t \odot f^t \odot \left(1 - f^t\right) \tag{18}$$

$$\widehat{\delta o}^t = \delta o^t \odot o^t \odot \left(1 - o^t\right) \tag{19}$$

Equations (16)–(19) can be written in the matrix form as,

$$\delta z^t = \left[\widehat{\delta a}^t, \widehat{\delta i}^t, \widehat{\delta f}^t, \widehat{\delta o}^t\right]^T \tag{20}$$

and,

$$\delta I^t = W^t \odot \delta z^t \tag{21}$$

then,

$$I^t = \begin{bmatrix} x^t \\ h^{t-1} \end{bmatrix} \tag{22}$$

Based on equations (7), (20) and (21), the weight can be updated in the LSTM network by using equation (22) as follow,

$$\delta W^t = \delta z^t \odot \left(I^t\right)^T \tag{23}$$

## 3. Experimental studies

In this study, the proposed RNNs with stacked LSTM algorithms developed for the automatic delineation of ECG waveform signal morphology using the QTDB consisted of the following main steps: (1) extracting the raw data from the QT Database, (2) preprocessing consisting of noise cancellation using DWT, and (3) classifying the ECG waveforms using RNNs with bidirectional LSTM for P-waves, QRS complexes, T-waves, and isoelectric lines based on time duration. All the phases of the proposed method are presented in Fig. 2.

### 3.1. Dataset

In this study, we used the QT Database (QTDB). Raw ECG data were obtained from the well-known Physionet public dataset [42]. The QTDB consists of 105 ECG recordings taken over 15 min from two-channel Holter-ECG recordings, including various QRS and ST-T morphologies. All recording samples were taken at 250 Hz. The current database is an excellent source of varied and well-defined ECG data. The records were chosen primarily from among existing ECG databases, including 15 MIT-BIH Arrhythmia records, 6 MIT-BIH ST Change records, 13 MIT-BIH Supraventricular Arrhythmia records, 33 European ST-T records, 4 MIT-BIH Long-Term ECG records, 10 MIT-BIH Normal Sinus Rhythm records, and 24 BIH "Sudden Death" records. The total QTDB dataset comprises about 105 records, and the sample of raw data for the six databases can be seen in Fig. 3. All records consist of a signal with the files *record.dat*, *record.hea*, and *record.atr*, which were assigned as original annotations to the data from the QTDB. However, records of sudden death are excluded because the signal morphology is too varied. Only a complete waveform of ECG signals in P-waves, QRS complexes, and T-waves is utilized. Furthermore, this study only uses one-channel Holter-ECG recordings from QTDB.

### 3.2. Noise cancellation

Unfortunately, the vital signs drawn from signal morphologies monitored by ECG can become corrupted during acquisition by different types of artifacts or power line interference [43]. By removing different kinds of noise and artifacts, the ECG signals are improved. It is apparent that the removal of the noise from the signal facilitates the processing. The different frequency bands of the ECG signal make it a suitable
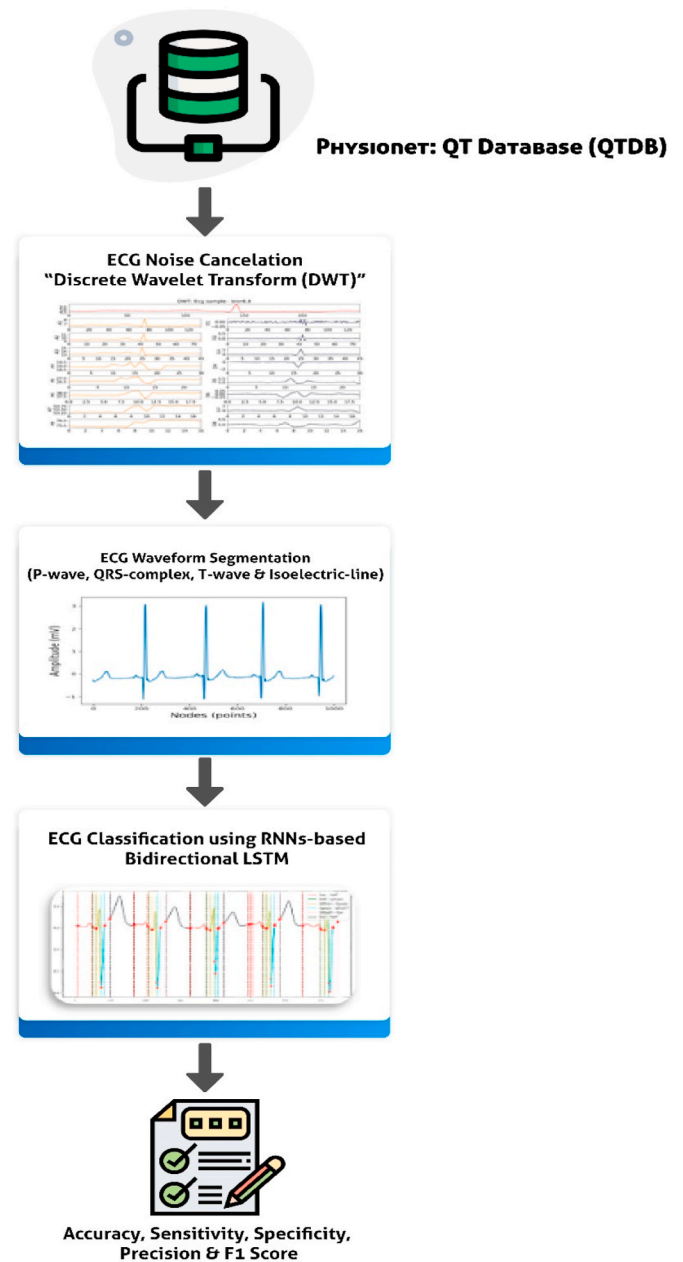


**Fig. 2.** Automatic delineation of ECG waveform signal morphology workflow.

candidate for multi-resolution decomposition using WT. The WT creates the possibility of selective noise filtering as a multi-resolution signal analysis tool, which contributes effectively to morphological observation. DWTs have been proposed with good results [5,13,28,44]. The DWT was applied to the process through a reconstruction of an ECG signal from a noisy signal. In the wavelet decomposition, a wavelet function was chosen and decomposed up to level *l*. The first step of the denoising procedure using the wavelet transform was selection by compression, stretching, or translation of the mother wavelet, which forms a collection of functions (or family of wavelets). In this study, Bior6.8 was selected because this wavelet function was thoroughly explored in previous research [44]. It produced high SNR compared to other wavelet functions used for denoising ECG signals [44] and provided a good result for ECG signal noise cancellation in our previous research [8].
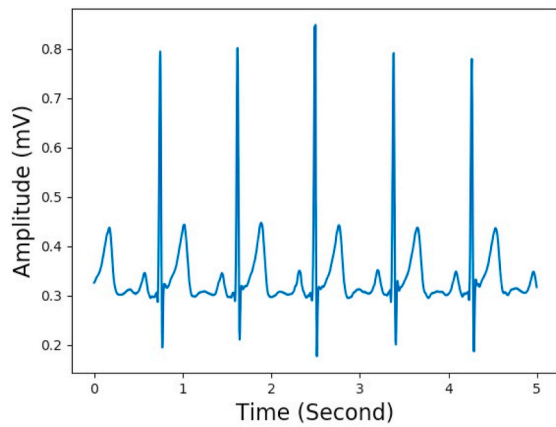
The next step was the degree of decomposition. The coefficient generated for a signal could have been altered previously, and the
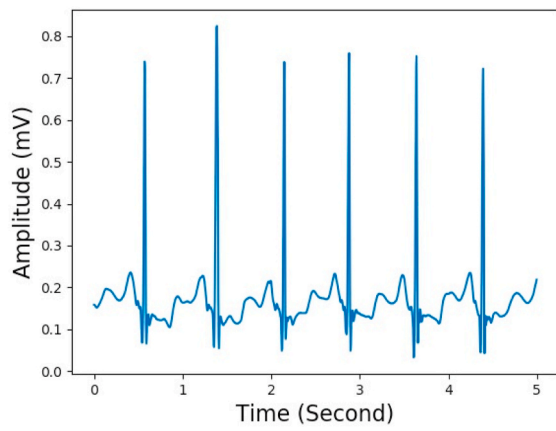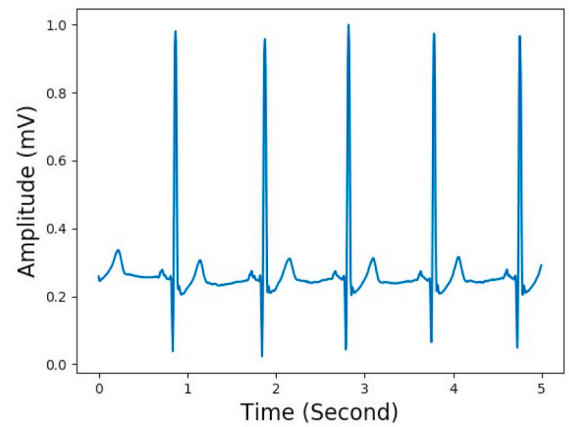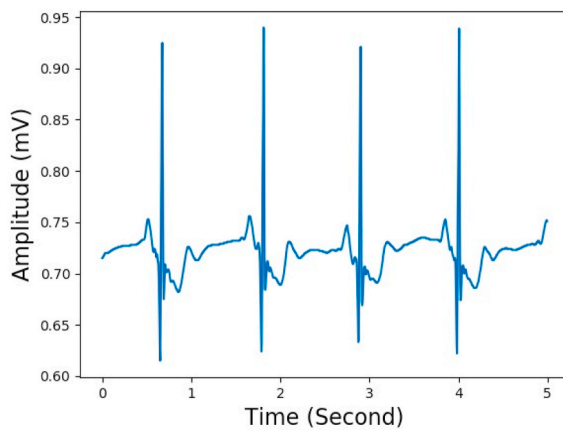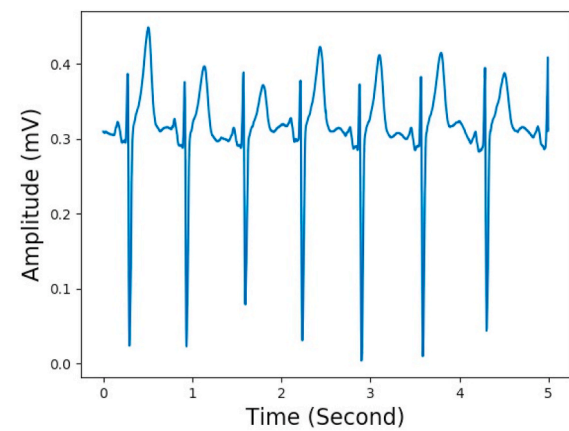
(a) MIT-BIH Arrhythmia
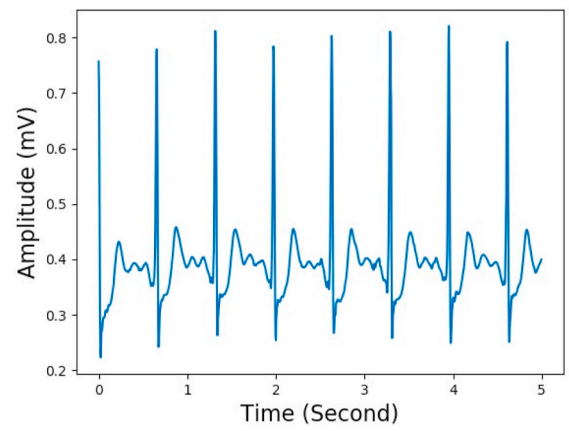
(b) MIT-BIH ST Change

(c) MIT-BIH Supraventricular
Arrhythmia

(d) MIT-BIH Normal Sinus
Rhythm

(e) European ST-T

(f) MIT-BIH Long-Term ECG

**Fig. 3.** Raw data from QT database.

reconstruction of the signal was meant to remove undesirable signal components. A wavelet function with *N* level was chosen, and wavelet decomposition of the signal at level *N* was calculated. The ECG signals were decomposed up to eight levels. Before the DWT model was utilized, seven experiments using 3, 4, 5, 6, 7, 9, and 10 levels of decomposition were performed. To achieve good performance, the wavelet decomposition process was repeated eight times within the symmetric structure. The result of the decomposition was filtered again by using the soft thresholding method (Equation (1)) with the universal threshold (Equation (2)). The first-level decomposition results were used to calculate the threshold value, and all levels of the 2D DWT component can be seen in Fig. 4. DWT only extracted clinically relevant markers from the data, which reduced data fed into the recurrent network algorithm by an order of magnitude while significantly increasing classification accuracy and execution time.

### 3.3. Cardiac waves duration classification

The cardiac wave series of P-waves, QRS complexes, and T-waves represents the duration of the ECG signal morphology. It is used to identify patients at risk for several symptoms. Features such as intervals, segment measurements, heart rates, and the frequency of R peaks have significant benefits for clinicians attempting to identify heart diseases. The algorithms designed must be applied to a delineated heartbeat that highlights several essential measurements of the electrical cardiac cycle.

Any noticeable changes occurring in the P-QRS-T lines indicate an irregularity in heartbeats. The physiology and morphology of ECG waveforms have frequently been used in clinical trials [4,45]. However, it is difficult to produce an algorithm that automatically produces a morphologic description for measuring the start and endpoint of the duration [3,14,15]. As a result, the automated delineation of ECG signal morphology is challenging.

In this paper, RNNs with bidirectional LSTM was proposed. By integrating input variables extracted from raw ECG data taken from the QTDB, this method was used to automatically identify the positions and magnitudes of the following durations, such as those of P-waves, QRS complexes, and T-waves. The QTDB provided the input to the WFDB *ecgpuwave* function, which provided us with the exact location of all the P, R, and T peaks in the signal [46]. The *ecgpuwave* output was written as a standard WFDB-format annotation file related to the specified annotator. It was utilized as a "ground truth" or label for the proposed ECG classification process. The cardiac wave classification was conducted with P-waves, QRS complexes, T-waves, and isoelectric lines. A fixed window size of 370 nodes for each sequence was utilized. The window size was sufficiently large to capture one heartbeat (from the start of P-wave 1 to the start of P-wave 2). After signal segmentation, we generated an index spanning from the start to the end of the P-wave, QRS complex, and T-wave positions based on the ground truth from *ecgpuwave*. The nodes' start-to-end index of the P-waves, QRS complexes, T-waves, and isoelectric lines had to be adjusted in units of
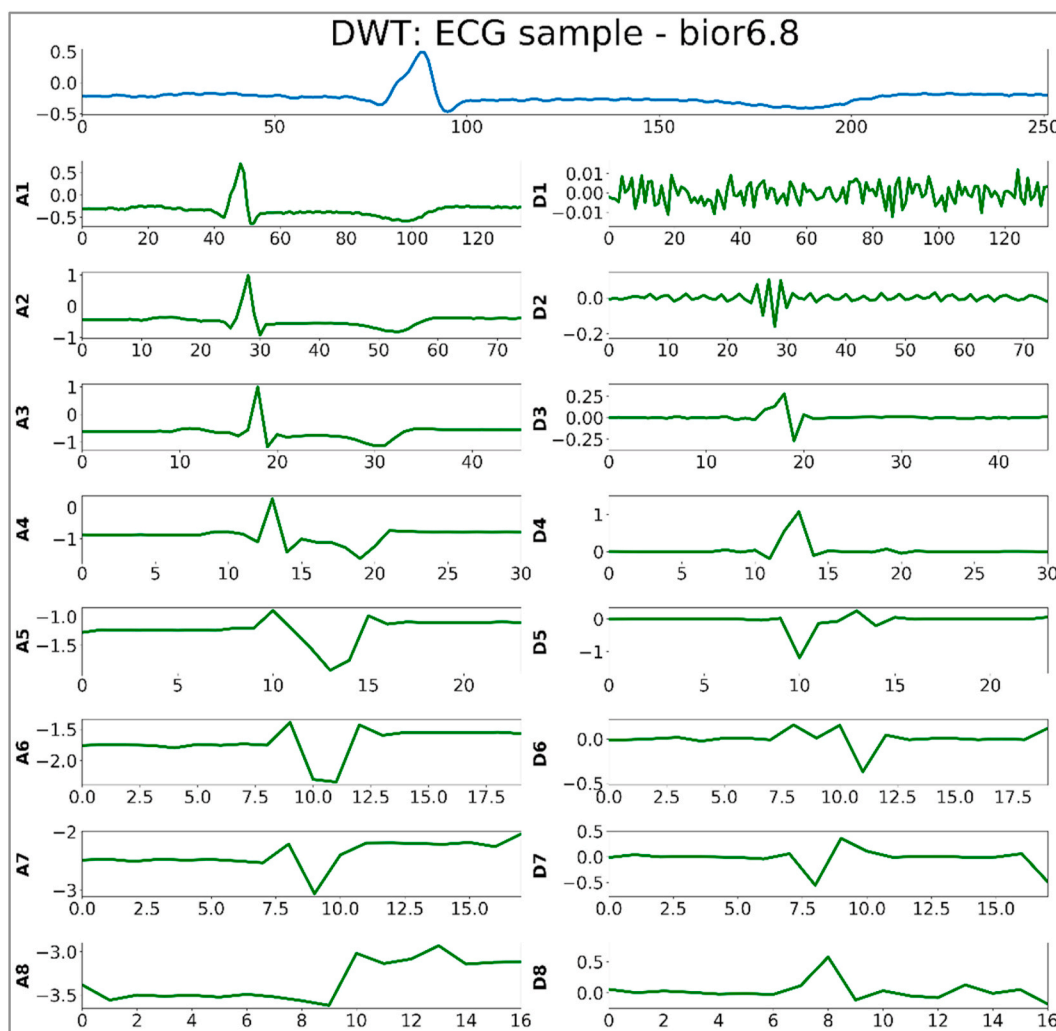


**Fig. 4.** ECG-wavelet for noise reduction in record sel100.dat (blue color: ECG raw data; green color: decomposition before and after thresholding). (For interpretation of the references to color in this figure legend, the reader is referred to the Web version of this article.)

seconds. All these duration points were sampled with a sampling frequency of about 250 Hz, and the duration in seconds (sec) could be calculated by utilizing the following equation [44],

$$Duration(\text{sec } ond) = \frac{po\text{int}samples}{samplingfrequency(Hz)} \quad (24)$$

After the preprocessing steps, a model for RNNs with bidirectional LSTM architecture was generated. The LSTM model was evaluated with both unidirectional and bidirectional passes to identify the best model. The bidirectional LSTM architecture with the hyperparameters presented in Table 1 was selected. The composition of the layer was 1 (one), in which each hidden activation function was either a Tanh-Sigmoid or an Adam optimizer. The output activation function was Softmax, which had a learning rate of 0.0001. Categorical cross-entropy was selected as a loss function.

The duration resulting from the proposed method was compared with the QTDB as annotated by *ecgpuwave* and manually annotated by an expert. In this study, not all records from the QTDB were manually annotated by an expert, as only 30 beats were contained in each record. Therefore, the QTDB records annotated by *ecgpuwave* became ground truth values, and the classification duration from the LSTM became a predicted value. Fig. 5 describes this process and presents the gap in the P-QRS-T wave between annotation (by *ecgpuwave* and experts) and prediction (from the proposed LSTM architecture).

## 4. Results and discussion

Data containing ten records from the QTDB of normal sinus rhythms became the baseline for P-wave, QRS complex, T-wave, and isoelectric line classification in the classification process. Using shuffle sampling, the classification process was divided into 90% in the training phase and 10% in the test phase. The total number of samples in the training set was 7.714, while the testing set used 858 samples. The testing set, as a validation set, was used to tune the hyper-parameters and determine the optimal number of models designed. To achieve an accurate result, we utilized a workstation with NVIDIA GeForce RTX 2080 and CuDNNLSTM. This GPU-accelerated deep neural network library supports training LSTM to classify the durations of all classes (P-waves, QRS complexes, T-waves, and isoelectric lines). As we stated above, the heartbeat segmentation contained one R-peak—from the start of one P-wave to the start of the next P-wave. In all signal recordings of normal sinus rhythms from the QTDB, the maximum length from the start of one P-wave to the start of the next P-wave was 370 nodes. If the length from the start of one P-wave to the start of the next P-wave did not achieve the maximum length, we set a condition requiring us to adjust that length; no padding was used. The results of LSTM performance for the QTDB are displayed in Table 2. The five performance metrics—i.e., accuracy, sensitivity, specificity, precision, and F1 score—were used for measuring the results [20,25]. These five metrics are commonly used for classification tasks in ECG signal processing [44,47,48]. The results were compared to P-wave, QRS complex, T-wave, and isoelectric line data annotated by *ecgpuwave* in the QTDB. For experiments, we also compared standard LSTM to bidirectional LSTM. The results showed that bidirectional LSTM had better performance. The standard (unidirectional) LSTM preserved information from the past and ran the inputs only in forward passes. The bidirectional phase ran inputs in forward and backward passes and preserved the information from both past and future. Table 2 displays the results of unidirectional and bidirectional

LSTM. As shown in Table 2, the average performance of bidirectional LSTM on the selected metrics was better than that of unidirectional LSTM. The average sensitivity increased from 97.96% to 98.74% using bidirectional LSTM. The other metrics also increased. Therefore, we selected the bidirectional LSTM model for P-wave, QRS complex, T-wave, and isoelectric line classification.

We have validated the proposed model through expert annotations on the bidirectional LSTM for the normal sinus rhythm database (.q1c) (refer to Table 3). Table 3 shows the results of the bidirectional LSTM model with expert annotations in QTDB (.q1c), which contained 30 non-sequential manually annotated beats in each record. There are 300 total manually annotated beats in the records from the normal sinus rhythm database. As we can see in Table 3, the average of all performance metrics decreased when compared to Table 2. For example, sensitivity went from 98.74% to 89.89%. This was possible because not all records with an expert annotation are manually annotated. Manual annotations by an expert are sometimes misplaced, and annotations are often missing along with the signal waveforms. The decision to seek expert annotation was made about the time location of the fiducial point. Unfortunately, in *ecgpuwave*, annotation is detected using the differentiated threshold method, not the fiducial point. This can affect the exact locations of all the P, R, and T peaks from the bidirectional LSTM learning model. For P-waves, the accuracy and precision were 99.24% and 99.27%, respectively. The sensitivity only reached 89.93%. The sensitivity of the QRS complex achieved 92.55%; however, the precision decreased, at only 88.81%. The worst validation results were for the T-waves, with a sensitivity of 79.44% and an F1-score of 87.79%.

The proposed bidirectional LSTM architecture was also trained in an abnormal QT database. For example, it was trained on MIT-BIH Arrhythmia, MIT-BIH ST Change, MIT-BIH Supraventricular Arrhythmia, European ST-T, and MIT-BIH Long-Term ECG (refer to Table 4). For MIT-BIH Arrhythmia, the average accuracy, sensitivity, specificity, precision, and F1-score values were 99.31%, 97.43%, 99.56%, 97.50%, and 97.47%, respectively. Commonly, for arrhythmia cases, the position of P-waves is an essential factor; for example, atrial fibrillation (AF) is one of the cardiac arrhythmias most frequent in the elderly population. The absence of a P-wave is one of the significant and clinically useful features for AF detection. This gives delineation of the P-wave considerable importance in clinical practice. It was also applied to MIT-BIH Supraventricular Arrhythmia, where we also achieved good performance, with an average accuracy of 99.26% for all waveforms. The average sensitivity, specificity, precision, and F1-score values were 97.31%, 99.51%, 97.60%, and 97.45%, respectively.

On the other hand, for the ST segment in particular, the position of the terminal QRS (J-point) and starting T-wave was crucial since the ST segment exhibited transient ST depression or elevation and was excerpted from long-term ECG recordings. For MIT-BIH ST Change and European ST-T, the average accuracy values were 99.31% and 99.35%, respectively. Unfortunately, in long-term ECG recordings, we obtained poor results on the average sensitivity, precision, and F1-score values, at 93.91%, 94.93%, and 94.38%, respectively. A signal recording that is too long could cause a normal T-wave to overlap with other T-wave classes—e.g., inverted, only upwards, only downwards, biphasic negative-positive, or biphasic positive-negative. Having multiple ECG signals of cardiac complexes could help the model find the cardiac wave relationship. In all cases, the proposed model could classify all categories of the ECG waveform component. The highest average accuracy in signal delineation was about 99.48% in MIT-BIH ST Change, and the

**Table 1**
The proposed architecture of bidirectional LSTM.

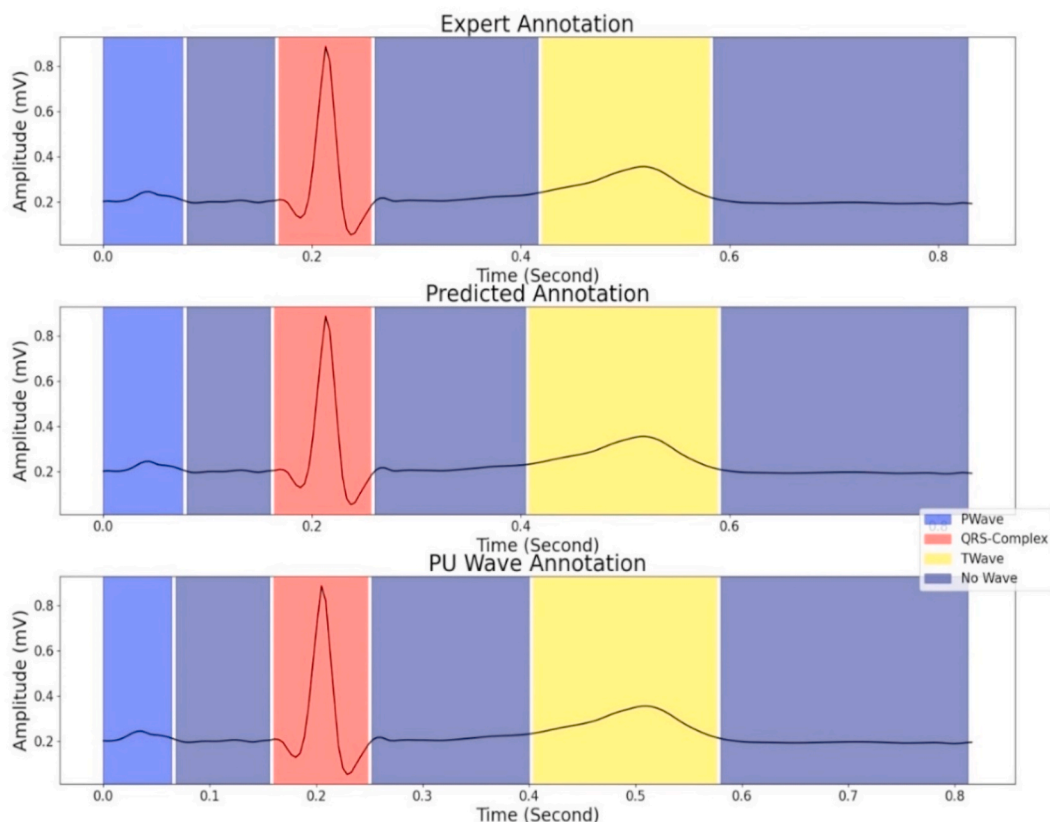| Method | Input Layer | Output Layer | Hidden Layer Neuron | Activation Function Hidden | Activation Function Output | Learning Rate | Loss Function | Batch Size | Epoch |
|---|---|---|---|---|---|---|---|---|---|
| Bidirectional LSTM | (370, 1) | 5 | 512 | Tanh-Sigmoid | Softmax | 0.0001 | Categorical Cross-Entropy | 8 | 300 |

**Fig. 5.** The sample of classification process for P-wave, QRS-complex, T-wave, and Isoelectric-line.

**Table 2**
LSTM performance of all classes based *ecgpuwave* notation in Normal Sinus Rhythm database.

| Method | Metrics | Performance (%) | | | | |
|---|---|---|---|---|---|---|
| | | P-wave | QRS-complex | T-wave | Isoelectric-line | Average |
| Unidirectional | Accuracy | 99.83 | 99.74 | 99.31 | 98.89 | 99.44 |
| LSTM | Sensitivity | 98.73 | 97.74 | 96.64 | 98.76 | 97.96 |
| | Specificity | 99.89 | 99.87 | 99.69 | 98.97 | 99.60 |
| | Precision | 98.39 | 98.14 | 97.88 | 98.34 | 98.18 |
| | F1-score | 98.56 | 97.94 | 97.26 | 98.55 | 98.07 |
| Bidirectional | Accuracy | 99.84 | 99.89 | 99.54 | 99.29 | 99.64 |
| LSTM | Sensitivity | 98.38 | 99.10 | 98.47 | 99.04 | 98.74 |
| | Specificity | 99.93 | 99.94 | 99.69 | 99.44 | 99.75 |
| | Precision | 99.00 | 99.24 | 97.92 | 99.10 | 98.81 |
| | F1-score | 98.69 | 99.17 | 98.20 | 99.07 | 98.78 |

**Table 3**
Bidirectional LSTM performance of all classes based expert annotation.

| Metrics | Performance (%) | | | | |
|---|---|---|---|---|---|
| | P-wave | QRS-complex | T-wave | Isoelectric-line | Average |
| Accuracy | 99.24 | 98.78 | 96.53 | 94.71 | 97.31 |
| Sensitivity | 89.93 | 92.55 | 79.44 | 97.64 | 89.89 |
| Specificity | 99.95 | 99.20 | 99.71 | 92.56 | 97.85 |
| Precision | 99.27 | 88.81 | 98.10 | 90.57 | 94.18 |
| F1-score | 94.37 | 90.64 | 87.79 | 93.97 | 91.69 |

**Table 4**
Bidirectional LSTM performance of all classes in abnormal database.

| Database | Average Performance (%) | | | | |
|---|---|---|---|---|---|
| | Accuracy | Sensitivity | Specificity | Precision | F1-score |
| MIT-BIH Arrhythmia | 99.31 | 97.43 | 99.56 | 97.50 | 97.47 |
| MIT-BIH ST Change | 99.48 | 97.83 | 99.68 | 98.08 | 97.95 |
| MIT-BIH Supraventricular Arrhythmia | 99.26 | 97.31 | 99.51 | 97.60 | 97.45 |
| European ST-T | 99.35 | 97.56 | 99.57 | 97.70 | 97.63 |
| MIT-BIH Long-Term ECG | 97.88 | 93.91 | 98.57 | 94.93 | 94.38 |

lowest accuracy in the MIT-BIH Long-Term ECG was 97.88%. Due to the raw data condition, in which the two signals were different, the Long-Term signal had more noise compared to ST Change. The overall results of the abnormal QTDB trials indicated that the proposed delineation algorithm exhibited a performance above 93% in identifying the ECG signal morphology. The results for the P-waves, QRS complexes, and T-waves in abnormal conditions can be seen in Fig. 6.

**MIT-BIH Arrhythmia** (a)

**MIT-BIH ST Change** (b)

**MIT-BIH Supraventricular Arrhythmia** (c)

**European ST-T** (d)
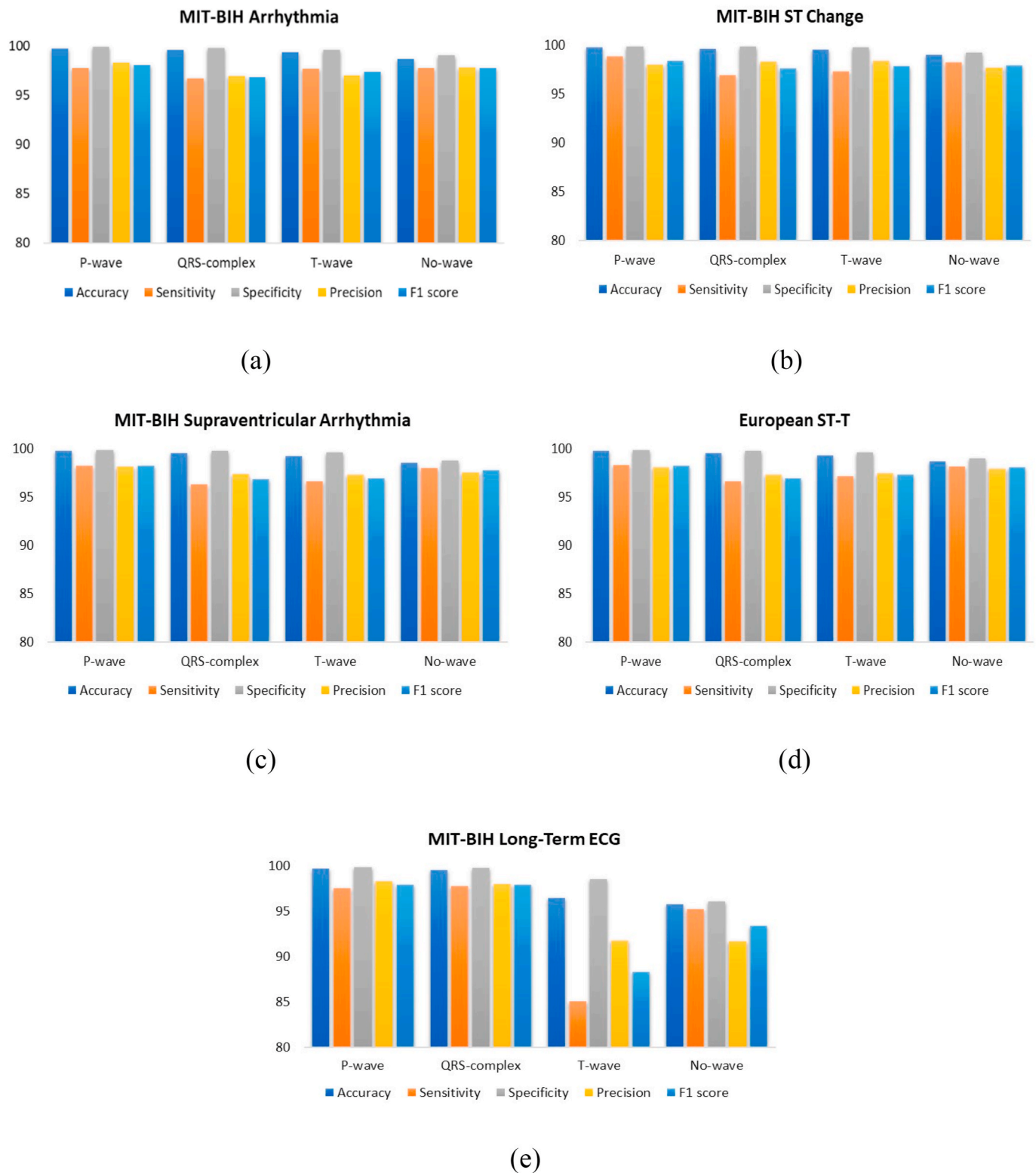
**MIT-BIH Long-Term ECG** (e)

**Fig. 6.** The performances of P-wave, QRS-complex, T-wave, and Isoelectric-line in abnormal QTDB.

Furthermore, for evaluating the proposed model in normal and abnormal rhythms, we used a learning curve. The learning curve consisted of accuracy and loss curves that showed model learning performance over time (in epochs). After each update, during training, plots of the assessed results can be generated to display learning curves. The model can be evaluated on the training data set and on a holdout testing dataset. Reviewing the model's learning curves during training may help to identify learning issues, such as an underfit or overfit model, and assess if the training and testing datasets are acceptable to represent. Accuracy and loss curves were generated in each database to represent the comparison between bidirectional LSTM and annotated QTDB records. There were accuracy and loss curves associated with the QTDB databases (Fig. 7 (a) to (l)).

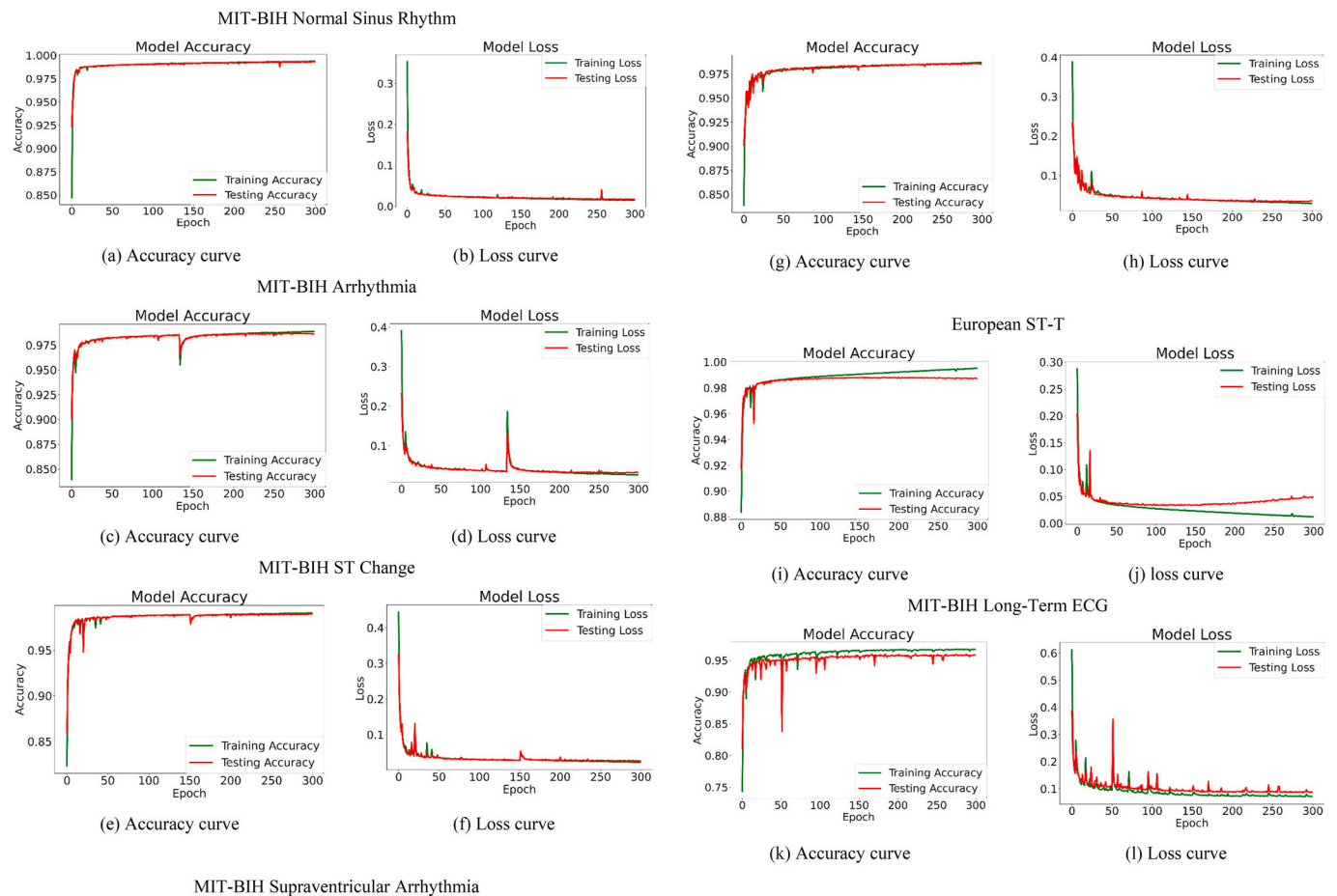It has previously been shown that the proposed RNNs with

**Fig. 7.** Accuracy and loss curve based on all waveform classes, MIT-BIH Normal Sinus Rhythm, MIT-BIH Arrhythmia, MIT-BIH ST Change, MIT-BIH Supraventricular Arrhythmia, European ST-T, and MIT-BIH Long-Term ECG.

bidirectional LSTM performed more accurately on all classes of ECG durations. Previous research explored ECG delineation for P-wave, QRS complex, and T-wave classification. The majority of the other studies focused on finding cardiac complexes with fiducial points rather than segmenting every ECG data point independently. The proposed method provides competitive accuracy in this field as well. Table 5 shows the accuracy of identifying cardiac waves using bidirectional LSTM regardless of segmentation. Hughes et al. [11] and Johannesen et al. [49] used the Hidden Markov Model (HMM) to solve ECG segmentation; they used wavelet-encoded and Markov models for automated ECG interval analysis. Lin et al. [6] proposed a conventional machine learning model that used a Bayesian approach for segmenting both P- and T-waves. Aside from this, Abrishami et al. [50] used DL in ECG segmentation. The method employed RNNs with bidirectional LSTM for segmenting P-waves, QRS complexes, and T-waves only. However, compared to studies [11,49], our proposed method outperformed that approach. With QRS complex classification in particular, our proposed algorithm can achieve an accuracy of 99.89% compared with the

previous studies (see Table 5). Table 5 shows the average accuracy for each of the models discussed. On the important task of accurately determining the P-wave, QRS complex, and T-wave values of QTDB signal morphologies, the RNNs with bidirectional LSTM significantly outperformed other methods and produced duration and QRS complex classifications for every signal morphology with excellent results. Altogether, using ECG signals from the QTDB, we achieved average accuracy values of 99.84%, 99.89%, 99.54%, and 99.29% for P-waves, QRS complexes, T-waves, and isoelectric lines, respectively.

Due to various normal and abnormal ECG signal spatial patterns, the traditional feature extraction methods, such as derivative-based methods, amplitude-based methods, etc., failed to extract various cardiac wave spatial formations. In contrast, RNNs with LSTM architecture using multilayer feature filters could extract more complex features from ECG signals automatically. These features could identify various ECG wave formations (P-waves, QRS complexes, and T-waves), delineate these waveform components, and detect key ECG waves. These results open up the possibility of making an impact on future research in

**Table 5**
ECG classification accuracy comparison.

| Authors | Methods | Dataset | Accuracy (%) | | | |
|---|---|---|---|---|---|---|
| | | | P-wave | QRS -complex | T-wave | Isoelectric-line |
| Hughes et al. [11] | Hidden Markov Model | 100 ECG waveforms | 05.50 | 79.00 | 83.60 | – |
| Johannesen et al. [49] | Wavelet | QTDB | 85.60 | 89.70 | 92.80 | – |
| Lin et al. [6] | Bayesian | QTDB | 98.93 | – | 99.54 | – |
| Abrishami et al. [50] | Bidirectional LSTM | QTDB | 92.00 | 94.00 | 90.00 | – |
| **Proposed** | Bidirectional LSTM | QTDB | 99.84 | 99.89 | 99.54 | 99.29 |

cardiology.

Although the results look promising, there are some limitations of our study:

- We used QTDB ground truths annotated by the *ecgpuwave* (by machine) due to the limited ECG delineations manually annotated by experts (cardiologists).
- We only classified T-waves as normal and ignored the other T-wave classes—namely, inverted, only upwards, only downwards, biphasic negative-positive, or biphasic positive-negative.
- We did not validate the proposed model in other ECG delineation databases. The research was limited to the ECG waveform in QTDB; more datasets could achieve greater generalization.

## 5. Conclusion

ECG waveform delineation is a process for determining amplitudes and time intervals. That is a challenging task due to several factors, such as the low amplitude of P-waves, biphasic P, and T-waves. The previous beat of a P-wave can be missing or partially overlap with the T-wave; some waves are arrhythmic, with abnormal beats; and measurements of the end of T-waves are inherently subjective. Therefore, it can greatly benefit the medical community to provide an accurate, automated ECG delineation device that can provide reliability, consistency, and security in each measurement. In this study, the RNNs with bidirectional LSTM architecture was proposed to overcome such a problem through the automated delineation of ECG waveforms. The main process was divided into noise cancelation, duration segmentation, wave form-based duration time classification, and model evaluation—a complete set of experimental classifications using a well-known QTDB dataset with normal and abnormal conditions. The proposed model accomplished the automatic delineation of ECG signals based on annotated data from QTDB, *ecgpuwave*, and experts, with satisfactory results. The proposed model produces 99.64% accuracy throughout the whole experiment, 98.74% sensitivity, 99.75% specificity, 98.81% precision, and a 98.78% F1-score. As these tools were further developed with data annotated by experts, RNNs with bidirectional LSTM architecture could aid in the early detection and diagnosis of patients with several morphological abnormalities. In the future, the potential of this delineation should be employed in potential applications for automated P-wave, QRS complex, and T-wave detection. By using the proposed method for universal screening, we can further investigate abnormal morphologies.

## Author contributions

S.N. Conceptualization, supervision, and writing—original draft; A. E.T. Validation and Evaluation; A.D. Formal analysis, data preparation, resources, and writing—review & editing; M.N.R. Software and writing—review & editing; J.E. Data preparation, Software; F.F. Data analyst; B.T. Data analyst.

## Declaration of competing interest

The authors declare that they have no known competing financial interests or personal relationships that could have appeared to influence the work reported in this paper.

## Acknowledgments

## Appendix A. Supplementary data

Supplementary data to this article can be found online at https://doi.org/10.1016/j.imu.2020.100507.

## References

[1] Fleming JS. Interpreting the electrocardiogram. Springer Science & Business Media; 2012.

[2] V Exner D. Noninvasive risk stratification after myocardial infarction: rationale, current evidence and the need for definitive trials. Can J Cardiol 2009;25:21A–7A.

[3] Schram M, et al. Prediction of the heart rate corrected QT interval (QTC) from A novel, multilead smartphone-enabled ECG using A deep neural network. J Am Coll Cardiol 2019;73(9 Supplement 1):368.

[4] Hajimolahoseini H, Redfearn D, Krahn A. A deep learning approach for diagnosing long QT syndrome without measuring QT interval. In: Canadian Conference on artificial intelligence; 2019. p. 440–5.

[5] Yochum M, Renaud C, Jacquir S. Automatic detection of P, QRS and T patterns in 12 leads ECG signal based on CWT. Biomed Signal Process Contr 2016;25:46–52.

[6] Lin C, Mailhes C, Tourneret J-Y. P-and T-wave delineation in ECG signals using a Bayesian approach and a partially collapsed Gibbs sampler. IEEE Trans Biomed Eng 2010;57(12):2840–9.

[7] V'itek M, Hrubeš J, Kozumpl'ik J. A wavelet-based ECG delineation with improved P wave offset detection accuracy. Anal. Biomed. Signals Images 2010;20:160–5.

[8] Nurmaini S, et al. An automated ECG beat classification system using deep neural networks with an unsupervised feature extraction technique. Appl Sci 2019;9(14): 2921. https://doi.org/10.3390/app9142921.

[9] Nurmaini S, et al. Deep learning-based stacked denoising and autoencoder for ECG heartbeat classification. Electronics 2020;9(1):135. https://doi.org/10.3390/electronics9010135.

[10] Schreier G, Hayn D, Lobodzinski S. Development of a new QT algorithm with heterogenous ECG databases. J Electrocardiol 2003;36:145–50.

[11] Hughes NP, Tarassenko L, Roberts SJ. Markov models for automated ECG interval analysis. In: Advances in neural information processing Systems; 2004. p. 611–8.

[12] Graff C, et al. Covariate analysis of QTc and T-wave morphology: new possibilities in the evaluation of drugs that affect cardiac repolarization. Clin Pharmacol Ther 2010;88(1):88–94.

[13] Saxena SC, Kumar V, Hamde ST. Feature extraction from ECG signals using wavelet transforms for disease diagnostics. Int J Syst Sci 2002;33(13):1073–85.

[14] Bisgin H, Kilinc OU, Ugur A, Xu X, Tuzcu V. Diagnosis of long QT syndrome via support vector machines classification. J Biomed Sci Eng 2011;4:264. 04.

[15] Brishty FP, Akhter S. Detection of drug-induced QT Syndrome from ECG using machine learning techniques. In: 2018 10th international Conference on Electrical and computer engineering. ICECE); 2018. p. 46–9.

[16] Nygårds M-E, Sörnmo L. Delineation of the QRS complex using the envelope of the ECG. Med Biol Eng Comput 1983;21(5):538–47.

[17] LeCun Y, Bengio Y, Hinton G. "Deep learning," *Nature* 2015;521(7553):436.

[18] Nurmaini Siti, Partan Radiyati Umi, Rachmatullah Muhammad Naufal. Deep neural networks classifiers on the electrocardiogram signal for intelligent interpretation system. Sriwij. Int. Conf. Med. Sci. 2019;1246(1):12030.

[19] Darmawahyuni A. Coronary heart disease interpretation based on deep neural network. Comput Eng Appl J 2019;8(1).

[20] Nurmaini S, et al. Robust detection of atrial fibrillation from short-term electrocardiogram using convolutional neural networks. Future Generat Comput Syst 2020. https://doi.org/10.1016/j.future.2020.07.021.

[21] Narula S, Shameer K, Omar AMS, Dudley JT, Sengupta PP. Machine-learning algorithms to automate morphological and functional assessments in 2D echocardiography. J Am Coll Cardiol 2016;68(21):2287–95.

[22] Rogers JG. Defining and refining heart failure risk stratification to optimize patient selection for cardiac transplantation. Am Heart Assoc; 2013.

[23] Gacek A, Pedrycz W. ECG signal processing, classification and interpretation: a comprehensive framework of computational intelligence. Springer-Verlag London Limited, Springer Science & Business Media; 2011.

[24] Attia ZI, et al. Noninvasive assessment of dofetilide plasma concentration using a deep learning (neural network) analysis of the surface electrocardiogram: a proof of concept study. PloS One 2018;13(8):e0201059.

[25] Darmawahyuni A, Nurmaini S, Yuwandini M, Rachmatullah MN, Firdaus F, Tutuko B. Congestive heart failure waveform classification based on short time-step analysis with recurrent network. Informatics Med. Unlocked 2020:100441.

[26] Darmawahyuni A, Nurmaini S, Caesarendra W, Bhayyu V, Rachmatullah MN. And others, "deep learning with a recurrent network structure in the sequence modeling of imbalanced data for ECG-rhythm classifier. Algorithms 2019;12(6):118. https://doi.org/10.3390/a12060118.

[27] Peimankar A, Puthusserypady S. An ensemble of deep recurrent neural networks for p-wave detection in electrocardiogram. In: ICASSP 2019-2019 IEEE international Conference on acoustics, Speech and signal processing. ICASSP); 2019. p. 1284–8.

[28] de Oliveira BR, Duarte MAQ, de Abreu CCE, Vieira Filho J. A wavelet-based method for power-line interference removal in ECG signals. Res. Biomed. Eng. 2018;34(1):73–86.

[29] Li C, Zheng C, Tai C. Detection of ECG characteristic points using wavelet transforms. IEEE Trans Biomed Eng 1995;42(1):21–8.

[30] Bahoura M, Hassani M, Hubin M. DSP implementation of wavelet transform for real time ECG wave forms detection and heart rate analysis. Comput Methods Progr Biomed 1997;52(1):35–44.

[31] Mart'inez JP, Almeida R, Olmos S, Rocha AP, Laguna P. A wavelet-based ECG delineator: evaluation on standard databases. IEEE Trans Biomed Eng 2004;51(4): 570–81.

[32] Manikandan MS, Dandapat S. Wavelet-based electrocardiogram signal compression methods and their performances: a prospective review. Biomed Signal Process Contr 2014;14:73–107.

[33] Caesarendra W, Wijaya T, Tjahjowidodo T, Pappachan BK, Wee A, Roslan MI. Adaptive neuro-fuzzy inference system for deburring stage classification and prediction for indirect quality monitoring. Appl Soft Comput 2018;72:565–78.

[34] Awal MA, Mostafa SS, Ahmad M, Rashid MA. An adaptive level dependent wavelet thresholding for ECG denoising. Biocybern. Biomed. Eng. 2014;34(4):238–49.

[35] Abbaspour S, Gholamhosseini H, Linden M. Evaluation of wavelet based methods in removing motion artifact from ECG signal. In: 16th nordic-baltic Conference on biomedical engineering; 2015. p. 1–4.

[36] Wang Z, Zhu J, Yan T, Yang L. A new modified wavelet-based ECG denoising. Comput. Assist. Surg. 2019:1–10. https://doi.org/10.1080/ 24699322.2018.1560088.

[37] Marini F, Bucci R, Magr\'\i AL, Magr\'\i AD. Artificial neural networks in chemometrics: history, examples and perspectives. Microchem J 2008;88(2): 178–85.

[38] Yildirim Ö. A novel wavelet sequence based on deep bidirectional LSTM network model for ECG signal classification. Comput Biol Med 2018;96:189–202. https:// doi.org/10.1016/j.compbiomed.2018.03.016.

[39] Darmawahyuni A, Nurmaini S. Deep learning with long short-term memory for enhancement myocardial infarction classification. and others. In: 2019 6th international Conference on instrumentation, control, and automation. ICA); 2019. p. 19–23. https://doi.org/10.1109/ICA.2019.8916683.

[40] Hochreiter S, Schmidhuber J. Long short-term memory. Neural Comput 1997;9(8): 1735–80. https://doi.org/10.1162/neco.1997.9.8.1735.

[41] Zen H, Sak H. Unidirectional long short-term memory recurrent neural network with recurrent output layer for low-latency speech synthesis. In: Acoustics, Speech and signal processing (ICASSP). IEEE International Conference on; 2015. p. 4470–4. 2015.

[42] Laguna P, Mark RG, Goldberg A, Moody GB. A database for evaluation of algorithms for measurement of QT and other waveform intervals in the ECG. In: *Computers in cardiology* 1997; 1997. p. 673–6.

[43] Wang J, Ye Y, Pan X, Gao X. Parallel-type fractional zero-phase filtering for ECG signal denoising. Biomed Signal Process Contr 2015;18:36–41. https://doi.org/ 10.1016/j.bspc.2014.10.012.

[44] Qin Q, Li J, Zhang L, Yue Y, Liu C. Combining low-dimensional wavelet features and support vector machine for arrhythmia beat classification. Sci Rep 2017;7(1): 6067.

[45] Lyon A, Mincholé A, Mart\'\inez JP, Laguna P, Rodriguez B. Computational techniques for ECG analysis and interpretation in light of their contribution to medical advances. J R Soc Interface 2018;15(138):20170821.

[46] Sodmann P, Vollmer M, Nath N, Kaderali L. A convolutional neural network for ECG annotation as the basis for classification of cardiac rhythms. Physiol Meas 2018;39(10):104005.

[47] Sánchez FAR, Cervera JAG. ECG classification using artificial neural networks. J Phys Conf 2019;1221(1):12062.

[48] Huang M-L, Wu Y-S. Classification of atrial fibrillation and normal sinus rhythm based on convolutional neural network. Biomed. Eng. Lett. 2020. https://doi.org/ 10.1007/s13534-020-00146-9.

[49] Johannesen L, Grove USL, Sørensen JS, Schmidt ML, Couderc JP, Graff C. A wavelet-based algorithm for delineation and classification of wave patterns in continuous Holter ECG recordings. In: 2010 Computing in cardiology; 2010. p. 979–82.

[50] Abrishami H, Han C, Zhou X, Campbell M, Czosek R. Supervised ECG interval segmentation using LSTM neural network. In: Proceedings of the international Conference on bioinformatics & computational biology. BIOCOMP); 2018. p. 71–7.